Color Constancy based on Image Similarity via Bilayer Sparse Coding

Bing Li[1], Weihua Xiong[2], Weiming Hu[1]

[1] NLPR,Institute of Automation,CAS,Beijing, 100190, China
[2] Omnivision Corporation, Sunnyvale, California, 95054, USA
Email:bli@nlpr.ia.ac.cn

Abstract. Computational color constancy is a very important topic in computer vision and has attracted many researchers' attention. Recently, lots of research has shown the effects of high level visual content information for illumination estimation. However, all of these existing methods are essentially combinational strategies in which image's content analysis is only used to guide the combination or selection from a variety of individual illumination estimation methods. In this paper, we propose a novel bilayer sparse coding model for illumination estimation that considers image similarity in terms of both low level color distribution and high level image scene content simultaneously. For the purpose, the image's scene content information is integrated with its color distribution to obtain optimal illumination estimation model. The experimental results on two real-world image sets show that our algorithm is superior to other prevailing illumination estimation methods, even better than combinational methods.

1 Introduction

The color signals of any object from an imaging device are determined by three factors: the color of light incident on the scene, the surface reflectance of the object, and sensor sensitivity function of the camera [1] [2]. Therefore, the color of same surface will usually appear differently under varying light sources. In contrast, the human beings have the ability to "see" a surface as having the same color independent of variations of the illumination, which is called "Color Constancy" [3]. Computational color constancy is targeted for providing the same sort of color stability in the context of computer vision [4], and its central issue is to build up an optimal illumination color estimation model.

Illumination estimation is actually an ill-posed problem and cannot be solved without any assumption. It has been an active research topic in both scientific community and imaging industry for several decades. Most early studies treat an image as a bag of pixels with RGB values and give out the illumination estimation model without considering the underlying semantic content expressed by the pixels' arrangement. We name these methods as "Data Driven Estimation Methods"(DD). Some of them, such as Grey World (GW)[5], maxRGB [6], Shades of Grey (SoG)[7], and Edge-based method [8], predefine fixed models

based on certain hypotheses for all images; while the others, including Color-by-Correlation (C-by-C) [9], Neural Networks based method (NN) [10], Support Vector Regression based method (SVR) [11], Gamut Mapping [12] etc, learn the optimal estimation model on the 2D/3D chromaticity space through a training procedure. Once the model is fixed in a DD method, the light colors of all the test images are computed out using the same model. Therefore, these methods are effective only when the distribution of colors within the image fits the assumed model.

Recent years have witnessed a rise in applying image content analysis in illumination estimation. We name these methods as "Content Driven Estimation Methods" (CD). So far, all the existing CD methods are essentially combinational methods [13] that generally contain two steps: (1) applying several individual estimation models (rather than only one) on the same image, (2) then selecting the best estimate or combining their outputs based on the image's content characteristics. Previous efforts in this area include the work of Gijsenij [14], which selects the most appropriate estimation method based on natural image texture statistics and scene semantics (NIS). Lu et al. [15] use 3D stage geometry model (SG) to divide images into different geometrical regions, and select appropriate estimations per depth layer or geometrical section. Bianco et al. [16] propose to use the indoor-outdoor scene classification for choosing the most appropriate estimation method. Weijier et al. [17] model an image as a mixture of semantic classes, such as sky, grass, road, and building, evaluate several different illumination estimations on the likelihood of its semantic content in correspondence with prior knowledge of the world, and produce the final output that results in the most likely semantic composition of the image. Although these methods have shown that high level scene content is useful for illumination estimation [13], they are inevitably affected by selected individual methods and automatically visual content analysis, in which the latter one itself, such as 3D stag classification or indoor-outdoor classification, is another difficult computer vision problem.

In this paper, we model illumination estimation as an image similarity problem and propose a novel bilayer sparse coding model that considers low level color distribution and high level scene category simultaneously. Our work is primarily inspired by two hypotheses: (1) The images with similar color distributions are preferable to be captured under the similar light colors; and (2) the scenes belonging to the same high level category have the similar illumination conditions [16]. This is because the varying range of light colors in a certain type of scene is often limited. For example, indoor lights tend to be red; while outdoor lights are mostly bluish. The first hypothesis has been validated in many DD methods that train estimation model using color chromaticity histogram. The second one has also been shown to be effective in some CD methods [14][15][16]. The approach described here is similar to what Bianco et al. [16] have done, but we do not explicitly classify the scene into predefined scene categories; then use the classification output to guide illumination estimation candidates' selection or combination. Instead, we integrate high level scene category analysis into the

illumination estimation procedure so as to avoid negative impact of false scene classification. Another contribution in the proposed method lies in, comparing with those DD methods that always use a prefixed (or learned) model for all the test images, that our model sparsely represents each test image by adaptively selecting training samples according to color and scene cues. The experiments on two real-world image sets show that our method outperforms other prevailing illumination estimation methods, even outperforms the CD combinational methods.

The remainder of this paper is organized as follows. In section 2, we briefly introduce the sparse coding technique. The details of the proposed method are presented in Section 3. Experimental results and further analysis are given out in Section 4. Section 5 concludes this paper.

2 Sparse Coding Preliminaries

Before introducing the details of our model, we start with a brief overview of sparse coding that is the basis of the proposed algorithm. Recently, much interest has been shown in computing linear sparse representation with respect to an overcomplete dictionary of the basis elements. The goal of sparse coding is to sparsely represent input vectors approximately as a weighted linear combination of a number of "basis vectors". Given an input vector $x \in R^k$ and basis vectors $\mathbf{U} = [u_1, u_2, ..., u_n] \in R^{k \times n}$, sparse coding aims to find a sparse vector of coefficients $\alpha \in R^n$, such that $x \approx \mathbf{U}\alpha = \sum_j u_j \alpha_j$. It equals to solving the following objective.

$$\min_{\alpha} \|x - \mathbf{U}\alpha\|_2^2 + \lambda \|\alpha\|_0 , \tag{1}$$

where $\|\alpha\|_0$ denotes the ℓ_0-norm, which counts the number of nonzero entries in a vector α. It is well known that the sparsest representation problem is NP-hard in general case. Fortunately, recent results [18] show that, if the solution is sparse enough, the sparse representation can be recovered by the following convex ℓ_1-norm minimization [18] as:

$$\min_{\alpha} \|x - \mathbf{U}\alpha\|_2^2 + \lambda \|\alpha\|_1 , \tag{2}$$

where the first term of Eq(2) is the reconstruction error, and the second term is used to control the sparsity of the coefficients vector α with the ℓ_1-norm. λ is regularization coefficient to control the sparsity of λ . The larger λ implies the sparser solution of λ. The sparse coding technique based on ℓ_1-norm has been widely applied in many practical applications, including face recognition, image classification, etc [18].

3 Bilayer Sparse Coding for Illumination Estimation

In this section, we firstly propose bilayer sparse coding model (BSC) for illumination estimation; then discuss color feature and scene feature used in BSC; and finally give out an optimization algorithm for BSC.

3.1 Bilayer Sparse Coding Model (BSC)

Sparse Coding for Color Similarity Analysis. Given N training images $I_1, ..., I_N$, the color feature vector of the image I_i is $C_i \in R^d$. Here, color feature C_i can be binarized 2D/3D chromaticity histogram that has been proved to be effective for many supervised color constancy algorithms [9][10][11]. For any test image I_y with color feature $C_y \in R^d$, we can linearly reconstruct its color feature using the training images under the sparse coding framework, as:

$$\min_{\gamma} \|C_y - \mathbf{C}\gamma\|_2^2 + \lambda \|\gamma\|_1 , \tag{3}$$

where $\mathbf{C} = [C_1, C_2, ..., C_N]$; $\gamma = [\gamma_1, \gamma_2, ..., \gamma_N]^T$ is a N-dimensional coefficient vector that indicates the reconstruction weight associated with each training image. From viewpoint of color gamut, the Eq(3) is actually to reconstruct the color gamut of the test image using color gamut of all the training images. The sparse code γ can also be viewed as the color correlation coefficient between I_y and each training image.

Sparse Coding for Scene Category Similarity Analysis. Besides color (or chromaticity) distribution, high level scene category cues embedded in the image can also improve the accuracy of illumination estimation [16]. Generally speaking, a typical type of scene is determined by a bag of certain objects and their co-occurrence relationships [19]. For example, the 'street' scene sometimes contains roads and buildings.

To model appearances of different objects in the scene, we segment each training image I_i into n_i objects, denoted as $I_i^1, I_i^2, ..., I_i^{n_i}$, then we have $n_1+n_2+...+n_N$ objects in the training image set in all. Each object I_i^k is represented by visual vocabulary histogram $v_i^k \in R^m$ that is gained from Bag-of-Words model (BOW) [20]; and all the objects in I_i^k are denoted as $V_i = [v_i^1, v_i^2, ..., v_i^{n_i}] \in R^{m \times n_i}$. The test image I_y is also segmented into n_y objects $I_y^1, I_y^2, ..., I_y^{n_y}$, their corresponding vocabulary histograms are represented as $v_y^1, v_y^2, ..., v_y^{n_y} \in R^m$. The scene category similarity analysis here is to reconstruct the n_y objects in the test image by using the $n_1 + n_2 + ... + n_N$ objects in the training images, as show in Fig. 1.

Considering co-occurrence property of objects in the same image, we should try to reconstruct the objects in the test image using those objects from the same training image. Therefore, we introduce the multi-task joint sparse representation based on $\ell_{1,2}$ norm [21]. The multi-task joint sparse representation can be regarded as a combinational model of group Lasso and multi-task Lasso by penalizing the sum of ℓ_2 norms of the blocks of coefficients associated with each covariate group (objects in each training image) across different reconstruction tasks (object reconstruction in the test image)[21].

For any test object I_y^j in the test image I_y, if $W_i^j \in R^{n_i}$ denotes the reconstruction coefficient associated with the objects $I_i^1, I_i^2, ..., I_i^{n_i}$ in the image I_i, we can use $W_i = [W_i^1, W_i^2, ..., W_i^{n_y}] \in R^{n_i \times n_y}$ to represent the reconstruction coefficient matrix of all the objects in I_y associated with all the objects in the image

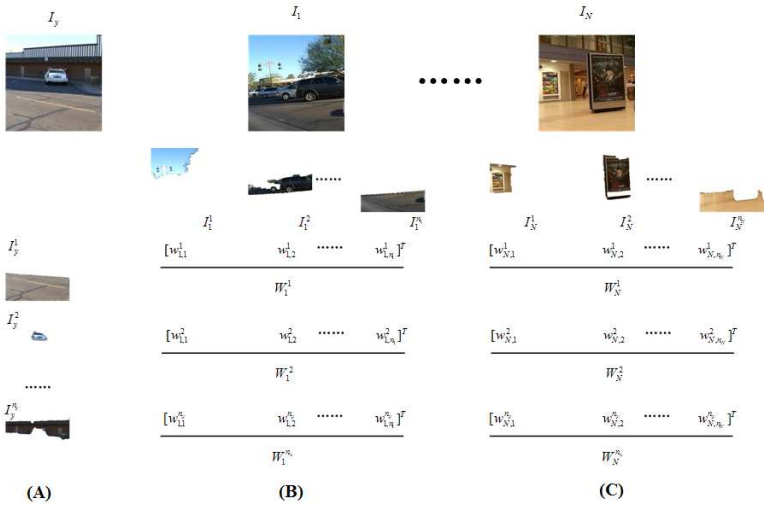

Fig. 1. Sparse reconstruction of image's scene content: (A) test images I_y and its segmented objects. (B) Training image I_1 and its segmented objects, $W_1^j, (j = 1, 2, ..., n_y)$ is a reconstruction coefficient vector of the j^{th} object in I_y associated with all the objects in I_1. (C) Training images I_N and its segmented objects, $W_N^j, (j = 1, 2, ..., n_y)$ is reconstruction coefficient vector of the j^{th} object in I_y associated with all the objects in I_N.

I_i . The details of corresponding relationship between objects and coefficient are shown in Fig. 1. The joint sparse representation of all the objects in the test image can be formulated as [21]:

$$\min_{\mathbf{W}} \sum_{j=1}^{n_y} \left\| v_y^j - \sum_{i=1}^{N} V_i W_i^j \right\|_2^2 + \beta \sum_{i=1}^{N} \|W_i\|_2^1, \tag{4}$$

where $\mathbf{W} = [W_1, W_2, ..., W_N]^T$ is the sparse coefficient matrix for all the objects in the test image; β is the regularization coefficient. The optimization problem in Eq(4), which is known as multi-task joint covariant selection in Lasso related research, can be effectively solved by $\ell_{1,2}$ mixed-norm Accelerated Proximal Gradient (APG) algorithm proposed by Yuan et al [21].

Bilayer Sparse Coding for Illumination Estimation(BSC). In order to integrate scene category information into illumination estimation model, a bilayer sparse coding model for illumination estimation is formulated to include similarity analysis on both color distribution and scene category, as:

Color Layer:

$$\begin{aligned} &\min_{\gamma} \|C_y - \mathbf{C}\gamma\|_2^2 + \lambda \|\mathbf{D}\gamma\|_1 , \\ &\mathbf{D} = diag(f(\|W_1\|_2^1), f(\|W_2\|_2^1), ..., f(\|W_N\|_2^1)), \end{aligned} \tag{5}$$

Scene Layer:

$$\min_{\mathbf{W}} \sum_{j=1}^{n_y} \left\| v_y^j - \sum_{i=1}^{N} V_i W_i^j \right\|_2^2 + \beta \sum_{i=1}^{N} g(\|\gamma_i\|_1) \|W_i\|_2^1, \tag{6}$$

where

$$f(\|W_i\|_2^1) = \frac{\max\limits_{k=1..N}(\|W_k\|_2^1) - \|W_i\|_2^1}{\max\limits_{k=1..N}(\|W_k\|_2^1) - \min\limits_{k=1..N}(\|W_k\|_2^1)}, \tag{7}$$

$$g(\|\gamma_i\|_1) = \frac{\max\limits_{k=1..N}(\|\gamma_k\|_1) - \|\gamma_i\|_1}{\max\limits_{k=1..N}(\|\gamma_k\|_1) - \min\limits_{k=1..N}(\|\gamma_k\|_1)}. \tag{8}$$

From the formulation above, we can find that the function $f(\|W_i\|_2^1)$ and $g(\|\gamma_i\|_1)$ are the monotone decreasing functions. Their outputs are between $[0, 1]$ and can be viewed as the costs in sparse color reconstruction and sparse scene content reconstruction. In the color layer, it tends to select the images with lower $f(\|W_i\|_2^1)$ values, which is corresponding to the higher $\ell_{1,2}$ norm $\|W_i\|_2^1$ of the scene reconstruction coefficient W_i, to reconstruct the test image's color feature. Similarly, in the scene layer, it tends to select the images with lower $g(\|\gamma_i\|_1)$, which is corresponding to the higher ℓ_1 norm $\|\gamma_i\|_1$ of the color reconstruction coefficient γ_i, to reconstruct the test image's scene content. Comparing Eq(5) with Eq(3) can tell us that the γ in BSC model contains not only color correlation but also scene content correlation information. The optimization of the BSC model will be discussed in section 3.3.

Illumination Estimation. The coefficient γ in Eq(5), which represents the correlation between the test image and all training images, is used for illumination estimation. To remove the shading effect, the ground truth illumination color value $e_i = (R_i, G_i, B_i)^T$ of the training image I_i is mapped into 2D chromaticity space through: $l_i = \left(\frac{R_i}{R_i+G_i+B_i}, \frac{G_i}{R_i+G_i+B_i}\right)^T$. And the coefficient vector γ is also normalized by ℓ_1 norm as: $\hat{\gamma} = \frac{|\gamma|}{\|\gamma\|_1}$. So the final illumination chromaticity $l_y = (r_y, g_y)^T$ of the test image can be estimated as the weighted average of the illumination values of all the training images as:

$$l_y = \mathbf{L}\hat{\gamma}, \ \mathbf{L} = [l_1, l_2, ..., l_N] \tag{9}$$

3.2 Feature Extraction

This section discusses the feature extraction in the BSC model. In the color reconstruction layer, we consider 3D color space as [11]: two chromaticity values, defined as $(r, g)^T = \left(\frac{R}{R+G+B}, \frac{G}{R+G+B}\right)^T$, and one intensity value, defined as $L = (R + G + B)$. The chromaticity space $(r, g)^T$ is equally partitioned along

each component into 50 equal parts yields 2500 bins. The intensity L is quantized into 25 equal steps [11][22], so the 3D color histograms consist of 62,500 ($50 \times 50 \times 25$) bins [11]. Each image is represented as a binarized 3D chromaticity histogram, in which '1' or '0' indicates the presence or absence of the corresponding chromaticity and intensity in the image.Since $0 \leq r+g \leq 1$, a compact 3D chromaticity histogram can be obtained by discarding the space with $r+g > 1$.

In the scene layer, the SIFT descriptor [23] that is widely applied in scene classification, is used as object's visual feature under the Bag-of-Word (BoW) model [20]. In order to remove the reciprocity of the two layers, the grey scale SIFT descriptor is used . The dense SIFT descriptors are extracted with 8-pixel step for each image. Then all the SIFT descriptors in the training images are clustered as m visual words via K-Means scheme. Finally, each segmented region with the corresponding SIFT descriptors in it is represented as a m-dimensional visual words histogram $v_i^k \in R^m$ via BoW model.

Table 1. Pseudo-code for bilayer sparse coding optimization.

Algorithm 1: Optimization of bilayer sparse coding

1: **Input:** The color feature C_i and scene feature $V_i = [v_i^1, v_i^2, ..., v_i^{n_i}] \in R^{m \times n_i}$ of each training image, the color feature C_y and scene feature $V_y = [v_y^1, v_y^2, ..., v_y^{n_y}]$ of the test image,the regularization coefficient λ and β, the threshold ε.

2: Initialize $\mathbf{D} = diag(1, 1, ..., 1)$, solve γ in Eq(5) via the $\ell_{1,2}$ mixed-norm APG.

3: **Repeat**

Set $p = \gamma$.

For $i = 1 : N$ Do
Compute $g(\|\gamma_i\|_1)$.
End

Solve $\mathbf{W}$ in Eq(6) with $g(\|\gamma_i\|_1)$ via the $\ell_{1,2}$ mixed-norm APG algorithm.

For $i = 1 : N$ Do
Compute $f(\|W_i\|_2^1)$.
End

Solve γ in Eq(5) with $f(\|W_i\|_2^1)$ via the $\ell_{1,2}$ mixed-norm APG algorithm.

Until ($\|\hat{p} - \hat{\gamma}\| \leq \varepsilon$ or max iteration times are arrived).

4: **Output:** γ and $\mathbf{W}$.

3.3 Optimization for Bilayer Sparse Coding Model

The optimization in Eq(5) and Eq(6) is not straightforward. However, if the value of γ is fixed, the optimization in scene layer is just a multi-task joint sparse coding, which can be effectively solved via the $\ell_{1,2}$ mixed-norm Accelerated Proximal Gradient (APG) algorithm [21]. On the other hand, if the coefficient matrix $\mathbf{W}$ is given, the optimization in color layer is just a general sparse coding with a cost constrain that can also be solved by the $\ell_{1,2}$ mixed-norm APG. Consequently, we give an approximate iterative $\ell_{1,2}$ mixed-norm APG algorithm to optimize the bilayer sparse coding as shown in table 1.

At each iteration, the new values of γ or $\mathbf{W}$ is obtained for the next iteration. The $\|\hat{p} - \hat{\gamma}\| \leq \varepsilon$, which indicates the distance between successive solutions of γ, is the stopping condition of the iterations. The threshold ε is fixed as 0.05 in this paper.

4 Experiments

We evaluate the proposed BSC algorithm on two real-world image sets. The first one is provided by Gehler et al. [24][25] and subsequently reprocessed by Shi et al.[26] (denoted as Gehler-Shi set); the second one includes the real-world images captured from a digital video provided by Ciurea et al (denoted as SFU set) [27]. The BSC method is compared with both some leading DD methods, , including GW [5], maxRGB [6], SoG [7], Grey Edge ($\mathbf{e}^{0,13,2}$, $\mathbf{e}^{1,1,6}$, $\mathbf{e}^{2,1,5}$)[8], NN[10], SVR[11]; and some CD combinational methods, such as NIS[14], SG[15] and IO[16]. The parameter settings for NN, SVR are determined according to the settings in [10] and [13], respectively. The parameters in NIS, IO and SG are the same as those used in [13].The binarized 3D color histogram is also used in SVR method. There are three parameters that are regularization coefficients λ, β and number of visual words m in BoW need to be set in advance in the BSC algorithm. In order to simplify the parameter selection, we fix $\lambda = \beta = 0.1$, the number of visual word m is set to be 200, 400, 800, respectively. The JSEG algorithm[28] is used to segment each object in the image due to its flexibility in adjusting the number of regions. After segmentation, those regions whose areas are less than $1/20$ of the whole image will be removed. In order to further validate the effect of the scene category for illumination estimation, the single color layer in BSC (denoted as SSC) excluding any scene cue is also used in comparison. The matrix $\mathbf{D}$ in SSC is always fixed as $\mathbf{D} = diag(1, 1, ..., 1)$.

4.1 Error Measurement

The error measurements is one of the most important issues in experiments. For each image in the image sets, the ground truth chromaticity of the light source $e_a = (r_a, g_a, b_a)$ is known. To measure how close the estimated illumination resembles the true color of the light source, the angular error measurement, which is the angular distance between the estimated illumination chromaticity e_y= $(r_y, g_y, 1 - r_y - g_y)^T$ and the ground truth chromaticity e_a, is adopted

to evaluate the performances of diverse algorithms. The angular error function $angular(e_y, e_a)$ is defined as

$$angular(e_y, e_a) = \cos^{-1}\left(\frac{e_y \bullet e_a}{\|e_y\| \, \|e_a\|}\right), \tag{10}$$

where $e_y \bullet e_a$ is the dot product of e_y and the e_a ; and $\|\bullet\|$ indicates the Euclidean norm. To measure the performance of an algorithm on a data set, the median angular error is used. Alternatively, to provide more insight into the complete distribution of errors on an image set, we also compute the trimean on a data set. The trimean value introduced by Gijsenij et al [29] can be calculated as the weighted average of the first, second, and third quantile Q_1, Q_2 and Q_3, respectively:

$$Trimean = \frac{Q_1 + 2Q_2 + Q_3}{4}. \tag{11}$$

4.2 Experimental Results on the Gehler-Shi Set

The Gehler-Shi image set contains 568 images that are taken using two high quality DSLR cameras (Canon 5D and Canon1D) and includes a wide variety of indoor and outdoor shots. All the images were saved in Canon RAW format. Because the tiff images provided by Gehler et al [24] in this set were produced automatically, they contain clipped pixels that are non-linear (i.e., have gamma or tone curve correction applied) and include the effect of the camera's white balancing. To avoid these problems, Shi et al. [26] reprocessed the raw data and created almost-raw 12-bit Portable Network Graphics (PNG) format images. This results in a 2041×1359 (for Canon 1D) or 2193×1640 (for Canon 5D) linear images (gamma=1) in camera RGB space. Consequently, the reprocessed Gehler-Shi set is used in the following experiments.

Although the correlations among images in this set are much lower [24], the 3-fold cross-validation strategy is still conducted to avoid overfitting. Considering that all images in this set are named in the sequence in which they were taken and neighboring images in the sequence are more likely than others to be of similar scenes, we ordered them by their filenames and divide them into 3 subsets. The first two subsets each include 189 images and the remaining one includes 190 images. During the experiment, one subset is picked as test set; the other two are used as training set. This procedure is repeated 3 times with different test set selection, the overall performance is used as the final result. The final experimental results are shown in Table 2.

The results in Table 2 show that, among all the existing methods that are compared with the proposed method in the paper, SVR and IO obtain best performances in their corresponding categories. Our proposed method is always better than SVR, no matter what value m is set. Specially, the BSC method with $m = 800$ achieves the best performance; and its median and trimean errors are 2.06 and 2.71, which also outperform the IO method. The BSC methods with $m = 200$ and $m = 400$ are comparable to IO method. However, we should

Table 2. Comparison of performance of all competing methods on the Gehler-Shi image set. Bold font indicates the minimum in each category. The Do Nothing method always estimates the illuminate as being white ($r = g = b$). Its performance is a measure of the amount of variation in the illumination color occurring within the image set.

Category	Algorithm	Median	Trimean
Data Driven	Do Nothing	4.80	7.53
	GW	3.70	4.09
	SoG	4.59	6.01
	maxRGB	9.18	9.77
	$\mathbf{e}^{0,13,2}$	4.72	5.88
	$\mathbf{e}^{1,1,6}$	3.63	4.01
	$\mathbf{e}^{2,1,5}$	3.71	4.09
	NN	4.52	5.80
	SVR	**2.76**	**3.13**
Content Driven	NIS	2.26	2.89
	IO	**2.23**	**2.83**
	SG	2.69	3.18
Proposed	BSC($m = 200$)	2.49	3.11
	BSC($m = 400$)	2.28	2.90
	BSC($m = 800$)	**2.06**	**2.71**
	SSC	2.83	3.29

emphasize that IO is a combinational method [13], while the propose BSC is an individual method. In addition, we can find that the performances of the BSC method are much better than SSC method. The fact implies that high level scene category cues can indeed improve the illumination estimation. Furthermore, the SSC has the similar performance to SVR, which shows that the sparse coding technique is effective for illumination prediction.

4.3 Experimental Results on the SFU Set

The second image set is introduced by Ciurea et al. [27] which consists of more than 11,000 frames from videos. Since the images in this set are extracted from videos, there exists high correlation between nearby images. Re-sampling is necessary for objective evaluations. To this end, Bianco et al. [16] apply a video-based analysis to select the image to reduce the correlations. The frames which show redundancy in terms of visual content are removed and only the most representative are retained. After this procedure, 1,135 images with much lower correlations are picked out. Since a matte grey sphere ball is mounted onto the video camera to obtain the ground truth illumination of each image; in order to ensure that the grey ball has no effect on our results, all images are cropped on the right to remove the grey ball. The remaining images are 240×240 pixels.

Since the SFU set contains 15 subcategories from which images are taken in different places, the 15-fold cross-validation is adopted here, which is the same as used by Gijsenij et al. [14]. To ensure that the training and testing subsets would be truly distinct, the Bianco's resampling set is partitioned into 15 subsets

based on geographical locations. Then one subset is used for testing and the other 14 ones are used for training. This procedure is repeated 15 times. The overall performance is shown in Table 3.

Table 3. Comparison of performance of all competing methods on the SFU image set. Bold font indicates the minimum in each category. The Do Nothing method always estimates the illuminate as being white ($r = g = b$). Its performance is a measure of the amount of variation in the illumination color occurring within the image set.

Category	Algorithm	Median	Trimean
Data Driven	Do Nothing	6.84	7.40
	GW	6.64	7.06
	SoG	6.19	5.64
	maxRGB	5.26	6.06
	$\mathbf{e}^{0,13,2}$	5.55	5.80
	$\mathbf{e}^{1,1,6}$	5.10	5.46
	$\mathbf{e}^{2,1,5}$	5.24	5.50
	NN	4.86	5.20
	SVR	**4.38**	**5.04**
Content Driven	NIS	4.83	5.66
	IO	**4.22**	**4.96**
	SG	4.97	5.46
Proposed	BSC($m = 200$)	3.90	4.28
	BSC($m = 400$)	**3.78**	**4.27**
	BSC($m = 800$)	3.95	4.31
	SSC	4.57	5.20

The same as previous experiment, SVR and IO methods still occupy the best positions in their corresponding categories. The similar conclusion to previous experiment can also be obtained. The proposed BSC methods with different m values, whose median errors are even less than 4.00, still outperform all other methods; even have better performances than content driven combinational method IO. The fact that all the BSC methods outperform SSC further confirms the effect of scene category cues in illumination estimation.

Finally, let's review the potential benefits of high level scene content analysis in illumination estimation using two examples. The image shown in Fig. 2(A) is captured indoor. If we only consider color distribution via SSC, matching figures with three highest γ_i values are shown from Fig. 2(A1) to (A3). Two of them (Fig. 2(A2) and (A3)) come from different scene categories and bias the final illumination estimation. By contrast, if we add high level scene content analysis into BSC, all the images with three highest γ_i values are from similar indoor scenes, and the final estimation is much closer to the real value. Another example in Fig. 2(B) is an outdoor scene with 'road'. If image scene content is considered using BSC, three most correlated images are all outdoor scenes also with 'roads', whose contributions result in accurate illumination estimation. The

examples further indicate that the constraint of high level scene category in BSC can actually improve illumination estimation.

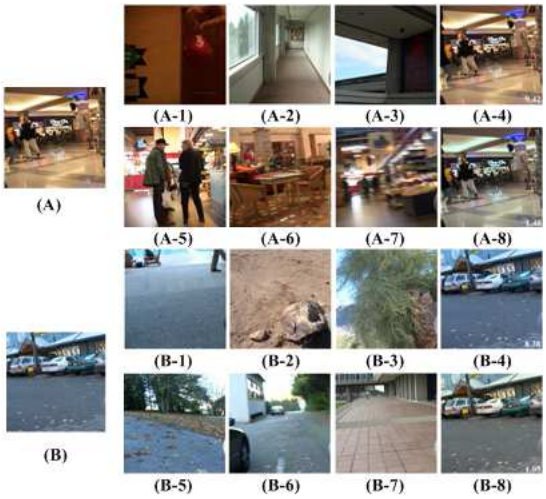

Fig. 2. Comparison between BSC($m = 400$) and SSC. (A)(B): test images. (A-1)-(A-3) and (B-1)-(B-3): images with three highest γ_i values associated with corresponding test images in SSC. (A-5)-(A-7) and (B-5)-(B-7): images with three highest γ_i values associated with corresponding test images in BSC. (A-4) and (B-4): corrected images using the estimates of SSC. (A-8) and (B-8): corrected images using the estimates of BSC. The angular errors (degree) in corrected images imply the accuracies of estimated illumination.

5 Conclusion

Image's high level content cue has been evidenced to be helpful in improving the illumination estimation for color constancy. However, nearly all the prevailing methods using high level content cues can be viewed as combinational methods that include two separate steps: applying several individual estimation models and combining their outputs through analyzing the test image's scene content. In this paper, we integrate image's color distribution and scene analysis into a unified framework, and propose a novel bilayer sparse coding model for illumination estimation problem. The experiments on two real-world image sets show that the mutually constrained combination can significantly improve the accuracy of illumination estimation and our proposed algorithm is superior to other prevailing methods, even better than the CD combinational methods.

References

1. Barnard, K., Cardei, V., Funt, B.: A comparison of computational color constancy algorithms-part 1: Methodology and experiments with synthesized data. IEEE TIP **11** (2002) 972–983
2. Barnard, K., Martin, L., Coath, A., Funt, B.: A comparison of computational color constancy algorithms-part 2: Experiments with image data. IEEE TIP **11** (2002) 985–996
3. Ebner, M.: Color Constancy. John Wiley & Sons (2006)
4. Barnard, K. Practical Colour Constancy. PhD thesis, Simon Fraser University, Canada, 1999.
5. Buchsbaum, G.: A spatial processor model for object colour perception. Journal of the Franklin Institute **310** (1980) 337–350
6. Land, E.H.: The retinex theory of color vision. Scientific American **237** (1977) 108–128
7. Finlayson, G., Trezzi., E.: Shades of gray and color constancy. In: Proc. of IS&T/SID Color Imaging Conference. (2004) 37–41
8. Weijer, J.V., Gevers, T., Gijsenij, A.: Edge-based color constancy. IEEE TIP **16** (2007) 2207–2214
9. Finlayson, G., Hordley, S., Hubel, P.: Color by correlation: A simple, unifying framework for color constancy. IEEE TPAMI **22** (2001) 1209–1221
10. Cardei, V., Funt, B., Barnard, K.: Estimating the scene illumination chromaticity using a neural network. JOSA A **19** (2002) 2374–2386
11. Xiong, W., Funt, B.: Estimating illumination chromaticity via support vector regression. Journal of Imaging Science and Technology **50** (2006) 341–348
12. Gijsenij, A., Gevers, T., Weijer, J.V.: Generalized gamut mapping using image derivative structuresfor color constancy. IJCV **86** (2010) 127–139
13. Li, B., Xiong, W., Hu, W.: Evaluating combinational color constancy methods on real-world images. In: Proc. of CVPR. (2011) 1929–1936
14. Gijsenij, A., Gevers, T.: Color constancy using natural image statistics and scene semantics. IEEE TPAMI **33** (2011) 687–698
15. Lu, R., Gijsenij, A., Gevers, T.: Color constancy using 3d scene geometry. In: Proc. of ICCV. (2009) 1749–1756
16. Bianco, S., Ciocca, G., Cusano, C., Schettini, R.: Improving color constancy using indoor-outdoor. IEEE TIP **17** (2010) 2381–2392
17. Weijer, J.V., Schmid, C., Verbeek, J.: Using high-level visual information for color constancy. In: Proc. of ICCV. (2007) 1–8
18. Wright, J., Ma, Y., Mairal, J., Sapiro, G.: Sparse representation for computer vision and pattern recognition. Proceedings of the IEEE **98** (2010) 1031–1044
19. Gokalp, D., Aksoy, S.: Scene classification using bag-of-regions representations. In: Proc. of CVPR. (2007) 1–8
20. Fei-Fei Li. Bag-of-Words model. Tutorial. In CVPR, 2007.
21. Yuan, X., Yan, S.: Visual classification with multi-task joint sparse representation. In: Proc. of CVPR. (2010) 3493–3500
22. Barnard, K., Martin, L., Funt, B.: Color by correlation in a three-dimensional color space. In: Proc. of ECCV. (2000) 375–389
23. Lowe, D.G.: Distinctive image features from scale-invariant keypoints. IJCV **60** (2004) 91–110
24. Gehler, P.V., Rother, C., Blake, A., Minka, T.: Bayesian color constancy revisited. In: Proc. of CVPR. (2008) 1–8

25. http://www.kyb.mpg.de/bs/people/pgehler/colour/.
26. Shi, L., Funt, B.: Re-processed Version of the Gehler Color Constancy Dataset of 568 Images. http://www.cs.sfu.ca/∼colour/data/.
27. Ciurea, F., Funt, B.: A large image database for color constancy research. In: Proc. of IS&T/SID Color Imaging Conference. (2003) 160–164
28. Deng, Y., Manjunath, B.S.: Unsupervised segmentation of color-texture regions in images and video. IEEE TPAMI **23** (2001) 800–810
29. Gijsenij, A., Gevers, T., Lucassen, M.P.: Perceptual analysis of distance measures for color constancy algorithms. JOSA A **26** (2009) 2243–2256